# MICROSTRUCTURAL CHARACTERIZATIONS AND STRENGTH DEVELOPMENT OF SELF-COMPACTING CONCRETE USING RICE HUSK ASH

F.R.P. PLANDO, J.T. MAQUILING

Ateneo Geophysics Research Laboratory, Physics Department,
Ateneo De Manila University, Katipunan Avenue, Quezon City 1108 Philippines
*Emails*: floyd.plando@obf.ateneo.edu; jmaquiling@ateneo.edu

*Received February 8, 2023*

*Abstract*. The conversion of waste and by-products into green building materials is gaining attention for a sustainable economy. Particularly, rice husk ash (RHA) is used as a precursor in self-compacting concrete due to its high pozzolanic activity. It also minimizes the use of conventional OPC as a primary binder during construction by exploiting its chemical features and characteristics as an alternative binding agent. Developing and mass-producing RHA as a cementitious material would lessen the carbon footprint that harms the environment. This study presents the compressive strength and microstructural characterizations of rice husk ash-based self-compacting concrete (RHA-SCC). The scanning electron microscope was utilized to determine the morphological images of RHA-SCC. The compressive strengths of 7, 28, and 90-day curing periods were also checked to relate how strength is developed from various sets of mixture proportions.

*Key words*: rice husk ash, microstructure, compressive strength.

## 1. INTRODUCTION

Rice is one of the world's most widely cultivated grains, second to wheat in the total cultivated land area [1]. The rice grain is usually located inside a protective shell called a rice husk that comprises almost one-fifth of its bulk grain weight [2]. Rice husk is a by-product of rice milling and usually throws away by disposing of it in a landfill or incinerating in a boiler to reduce its volume [3]. Calcining rice husk between 500–800°C produces rice husk ash, a highly pozzolanic material with highly porous particles, large external surface area, and low bulk unit weight. It has an amorphous mineral phase (partly semi-crystalline at a much higher temperature) and contains chemically reactive, high silica content.

Due to RHA's high pozzolanic activity, high specific surface area with low reaction time enhances cement hydration, improves mechanical properties and durability, and reduces cement porosity [4]. A study revealed that RHA-mixed cement paste contains a few quantities of calcium hydroxide (CH) owing to its pozzolanic activity. Meanwhile, due to the reactive $SiO_2$ content of RHA, it micro-fills the pores in between the cement grains. Combining RHA with cement lowers

its total porosity, increasing its packing density and enhancing the interfacial transition zone (ITZ) between the cement network and aggregates. Also, CH binds with the calcium silicate hydrate (CSH) reaction product, then subsequently decreases due to the secondary hydration reaction of RHA particles [5]. The remaining CSH gels fill the micro-pores of ITZ and improve the intermolecular interaction of the cement matrix and aggregates [6].

Some research provides techniques for studying the microstructure of concrete matrices. One of the widely used is through Scanning electron microscopy (SEM); it is a technique for visualizing the morphology of a sample in two dimensions (2D). Through this, it characterizes the solid phases in the microstructure of the concrete, allowing it to qualitatively determine the existing phases and reaction products in a 2D cross-section. Combining this technique with results from compressive strength performance would evaluate the cause of the strength development of RHA-SCC. This is an important assessment since various factors affect the quality and serviceability of the concrete structure.

In this paper, it aims to determine the specific mix proportions that would deliver the best compressive strength. This relates to what mineral phases and reaction products are visible that influence the strength development of the samples.

## 2. MATERIALS AND METHODS

### 2.1. SAMPLES

For the supplementary cementitious materials (SCM), the rice husk ash (RHA) used was collected from local rice millers in Laguna while Type I fly ash-blend ordinary Portland cement (OPC) was obtained from Cavite, confirming the specifications of ASTM C150-97. Table 1 presents both the chemical and physical properties of SCM.

The fine aggregate utilized in this work was locally siliceous fine sand from Porac, Pampanga with a fineness passing 9.5 mm. It has a specific gravity of 2.57, a bulk unit weight of 1571 $kg \cdot m^{-3}$, and a fineness modulus of 2.48. The coarse aggregate used is a ground basalt (also known as blue gravel) from Montalban, Rizal with a nominal size of 3/4” (19 mm) with a specific gravity of 2.83, bulk unit weight of 1636 $kg \cdot m^{-3}$, and materials finer than 75 μm of 0.19%.

RC Superconplas-SRW is a superplasticizer, retarder, and water reducer conforming to ASTM C94 Types D and G. It is a dark brown, liquid solution mixture of calcium and sodium lignosulphonates and concrete plasticizing resins in water, with a density of 1.12 kg/l. While RC Zeecon AEA is a liquid-type air-entraining admixture that complies with ASTM C260. It has a high concentration

of vinsol resin in water, creating a low viscosity and dispersing readily throughout the concrete.

*Table 1*

Physical and chemical properties of RHA and OPC

| Properties | RHA | OPC |
|---|---|---|
| Specific gravity | 1.17 | 3.12 |
| Absorption (%) | 12.4 | – |
| Fineness (75 µm, %) | 4.00 | 1.35 |
| Coefficient of uniformity ($C_U$) | 2.93 | 2.78 |
| Coefficient of curvature ($C_C$) | 1.09 | 1.44 |
| Color | Light grey | Grey |
| Chemical compositions (%) | | |
| $SiO_2$ | 93.55 | 28.45 |
| $Al_2O_3$ | 0.16 | 7.13 |
| $Fe_2O_3$ | 0.32 | 5.72 |
| $SiO_2 + Al_2O_3 + Fe_2O_3$ | 94.03 | 41.30 |
| $SO_3$ | 0.22 | 4.45 |
| CaO | 0.61 | 48.95 |
| $K_2O$ | 2.22 | 0.46 |
| $MnO_2$ | 0.24 | 0.10 |

### 2.2. SAMPLE PREPARATIONS AND PROPORTIONS

As pre-treatment measures for RHA, the sieving of collected batch samples was done by an electromagnetic shaker (SY-200, Xianxiang Karat Machinery) with a frame size of < 75 µm. The standard sieve duration ran for 10 min, allowing for vibration and segregation of the particles to the chosen size. The collected RHA samples were stored in a covered bucket.

The preparation of the alkali was 24 h before casting the mixture. This not only allows full depolymerization of $Na_2SiO_3$ in the solution, but also cools and matures it before mixing by reducing the heat liberation through the exothermic reaction of NaOH and water, and preventing the quick setting of cement and RHA during mixing. Cocktails were stored in polypropylene plastic containers since they are inert and non-reactive.

The researchers prepared fifteen different mix trials of RHA-SCC samples with different proportions of RHA as substitutions to OPC by mass, as presented in Table 2. The procedure of casting the mixture started by mixing first the aggregates for 2 min in an electric drum concrete mixer (model CML22B) with a wet mixed capacity of 60 l.

*Table 2*

Detailed mixed proportions of RHA-blend SCC

| S/N | SCM | | | | w/b | Aggregates (kg/m$^3$) | |
|---|---|---|---|---|---|---|---|
| | OPC (kg/m$^3$) | RHA (%) | RHA (kg/m$^3$) | RHA size (μm) | | Sand | Gravel |
| SC01 | 272 | 5 | 55 | unsieved | 0.45 | 1454 | 709 |
| SC02 | 242 | 10 | 180 | unsieved | 0.40 | 1508 | 599 |
| SC03 | 212 | 15 | 120 | unsieved | 0.35 | 1562 | 508 |
| SC04 | 272 | 5 | 55 | < 300 | 0.45 | 1454 | 578 |
| SC05 | 242 | 10 | 180 | < 300 | 0.40 | 1508 | 490 |
| SC06 | 212 | 15 | 120 | < 300 | 0.35 | 1562 | 755 |
| SC07 | 272 | 5 | 55 | < 125 | 0.45 | 1454 | 482 |
| SC08 | 242 | 10 | 180 | < 125 | 0.40 | 1508 | 599 |
| SC09 | 212 | 15 | 120 | < 125 | 0.35 | 1562 | 755 |
| SC10 | 272 | 5 | 55 | < 75 | 0.45 | 1454 | 709 |
| SC11 | 242 | 10 | 180 | < 75 | 0.40 | 1508 | 490 |
| SC12 | 212 | 15 | 120 | < 75 | 0.35 | 1562 | 620 |
| ‡SC13 | 272 | 0 | 0 | – | 0.45 | 1454 | 482 |
| ‡SC14 | 242 | 0 | 0 | – | 0.40 | 1508 | 714 |
| ‡SC15 | 212 | 0 | 0 | – | 0.35 | 1562 | 629 |

‡ control samples; all samples contained 312.4 ml of SP and 3.94 ml of AEA

### 2.3. TEST METHODS

The 7, 28, and 90-day compressive strengths of the hardened RHA-SCC samples were tested using a micro-computer controlled automatic compression tester (PILOT COMPACT Model: 50-C23C02) with parameters of 2000 kN capacity, and 50–100 psi/s loading rate. This process is according to the specification standards in ASTM C109. Partial substitution of OPC by RHA were 5, 10, and 15%, with RHA sizes of unsieved (as-received RHA) and sieved at < 75 μm. These parameters were checked to see how RHA substitutions, in terms of volume and size, influence the strength development within the RHA-SCC as time progressed. The water-to-binder ratio (*w*/*b*) varied to 0.35, 0.40, and 0.45.

Morphological and microstructure images were carried out using a scanning electron microscope (SEM, Hitachi TM-1000) operated at 15 kV accelerating voltage and sputtered using auto fine Platinum coater (JEOL JEC-3000 FC). The samples

were cut into thin disks and, eventually, mounted to ultra-low viscosity epoxy resin to seal the pores of the samples, avoiding moisture while discontinuing the hydration process.

## 3. RESULTS

Figure 1 exhibits the results of compressive strengths for 15 mixtures after 7, 28, and 90 day curing age. While SS/SH alkali ratio, SP dosage, and Si/Al ratio were kept constant, parameters such as the *w*/*b* ratio and volume fraction of RHA replacement vary, which may heavily influence the compressive strength of the hardened concrete. Each value denotes the average of three experimental observant ions. SC01 was observed to have the lowest compressive strength for all ages. There was also an increasing trend distinguished for samples for every three samples (*i.e.*, SC01-03, SC04-06, and so on), but varied in RHA replacement and size. High compressive strengths were obtained at samples with high RHA replacement and sieved at much smaller size fractions. The SC12 sample, which contained a *w*/*b* ratio of 0.35 and 15% RHA replacement, was recorded with the highest compressive strength at 7 days and was slightly comparable to the compressive strength of samples having the same *w*/*b* ratio and RHA replacement. This increasing trend continued until 90 days. At this higher age, all concrete samples produced the highest compressive strengths among all ages.

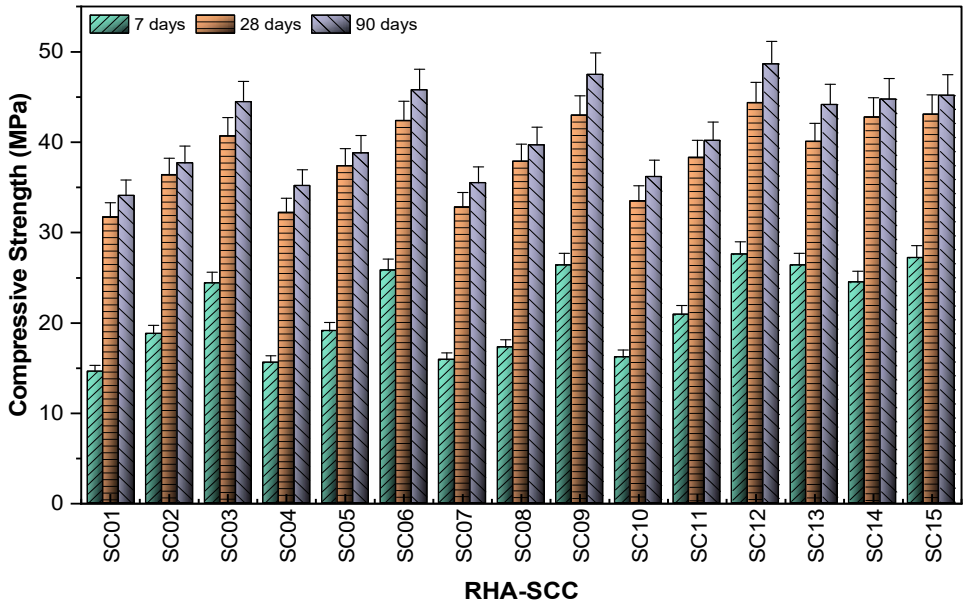


Fig. 1 – Compressive strengths of RHA-SCC at various curing periods.

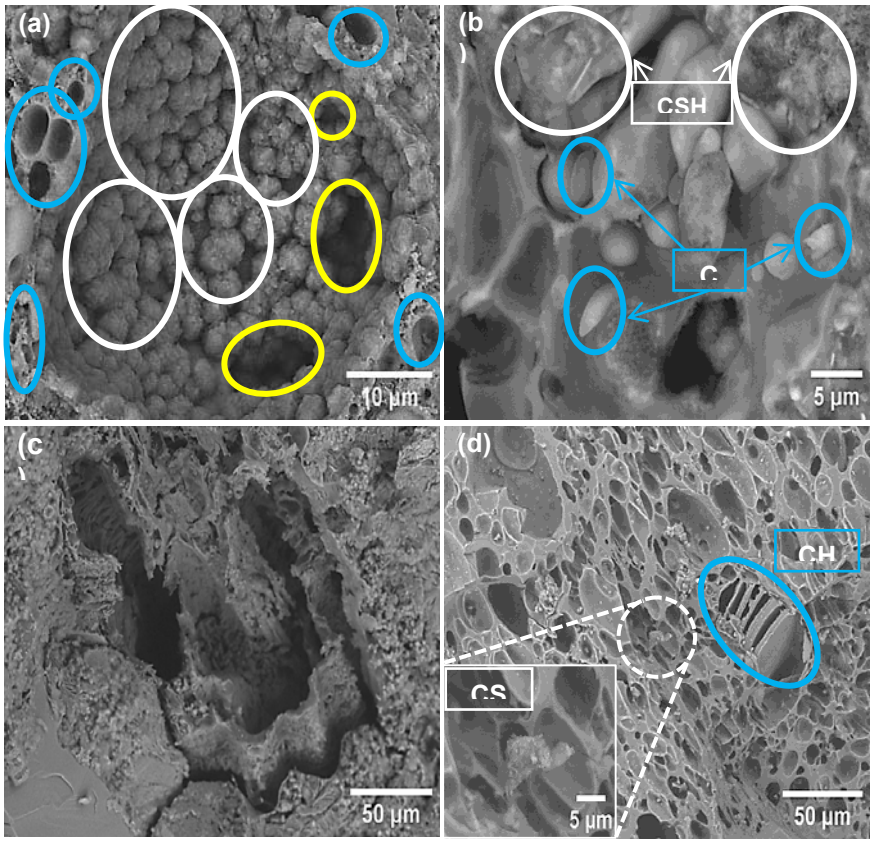


Fig. 2 – RHA-SCC sample microstructures showing: a) agglomeration of CSH (SC01); b) milky globular structure (SC12); c) unreacted RHA (SC04); d) honeycomb microstructure from unreacted RHA (SC10) (Color Online).

Surface morphologies of RHA-SCC samples at 28 days are shown from SEM images in Figs. 2 and 3. Figure 2a exhibits the agglomeration of the cementitious matrix formed inside the cavity. This microstructure is characterized by a porous surface, which consists of microreliefs (white circles) with an average size of 3 µm, microcavities (yellow circles), and capillary pores (blue circles) with an average size of 4 µm. Microreliefs are CSH gel reaction products from the combination of cement and RHA, and they display good adhesion with each other by forming globules as they get hydrated, assembled, and settled in the cavity. Aside from the hydration gel products, *i.e.*, CSH and CH, the cementitious matrix also consisted of capillary pores lying on the rim of the cavity. These are the remains of once water-filled voids [7]. A milky globular microstructure is exhibited in Fig. 2b, showing the presence of both CSH and CH gel products. From the micrograph, there are protuberant surface characteristics distinctive from the rest of the images and there are occurrences of microcavities. Since the cement particles are fully engaged with

RHA upon mixing, the formation of hydration gel products would be much easier because of the high porosity and SSA of the RHA, encouraging high moisture transport along the process [8]. Due to the weak physical behavior of RHA particles, a limitation in binder phase formation should be considered which contributes to the mechanical properties of the sample equated to the amount of unreacted RHA present in the concrete matrix. Figure 2c displays the magnified unreacted RHA seen in SC04, and this was also seen in SC01 and SC07 samples. This concludes that a higher rate of unreacted RHA in a sample yielded a lower compressive strength (Fig. 1). This loss in compressive strength may be due to the trapped unreacted siliceous particles in the voids, minimizing the egress of internal pressure. Such pressure buildup detriments the overall mechanical strength due to the produced internal microcracks, which were also spotted around the unreacted RHA of Fig. 2c. To assure the complete dissolution of RHA, a thorough mixture must be made in enhancing not only the strength but as well as the pozzolanic reactions of precursors to other SCM [9]. A honeycombed microstructure attached to the concrete matrix is seen in Fig. 2d. The honeycombed pores, with an average size of about 15 μm, are arranged in a crisscrossed pattern attached to the fibrillary plate of RHA. They are highly dependent on the grinding process, but independent of the calcination process. The magnification of the image sheet revealed the CSH attachments inside the holes and the integration of CH in the honeycombed microstructure (blue circles). This micrograph confirmed the porous structure and high surface area of SC07 sample inherent to the unreacted RHA morphology [10].

Figure 3a shows the formation of ettringite lying on a low-porosity surface of the concrete matrix. Ettringite is one of the main hydration components of OPC-blended concrete. It has a white, needle-like crystal morphology of calcium sulfoaluminate (CSA) hydrate origin, which plays a major part in the control of the setting. It typically develops when cement is hydrated as CSA is one of the cement clinkers. The chemical reaction between sulfate compounds, such as gypsum, and calcium aluminate sources forms the ettringite within a few minutes after it gets hydrated. Additional sulfate with contaminated mixing water, such as hard water, could significantly damage the microstructure of concrete by bulking up and creating microcracks [11]. Overall, ettringite only consumes 15% of solid volume in the microstructure properties. An interfacial transition zone (ITZ) is observed in the SC06 sample (Fig. 3b). The ITZ is the perturbed zone in the cement paste due to the occurrence of aggregates around it. It is known as the most important interface responsible for the mechanical strength and transport behavior of the concrete. From the micrograph, the formation of ITZ was due to the agglomeration of fine, hydrated grains with other reaction gel products of the concrete away from the coarse aggregate's surface, resulting in a "wall" effect. A highly heterogeneous and compacted cement matrix is dominated by CSH phase formation instead of CH, producing an improved compressive strength for SC06 [12]. Utilizing SCM for binary or ternary-blended binder, and examining the physical properties of the aggregate (*i.e.*, size, shape, and texture) may enhance the ITZ and its wall effect.

Figure 3c shows the RHA-SCC matrix from SC11 revealed the presence of CSH and CH products as the dominant reaction gel products in the sample. This suggests the consumption of CH and CSH was due to the pozzolanic reaction of both OPC and RHA. A CSH phase appeared in a reticular network, while the CH phase appearance was massive, platy crystals. Some voids also exist in the micrograph and can be accounted for by the matrix cracks, producing lower compressive strength of the sample. Another ITZ is seen from the RHA-SCC sample (SC05, Fig. 3d) and observed a gradual transition between the heterogeneous cement matrix and aggregate. The matrix consists of dominant CSH and CH gel products, and the chemical reactions between RHA and OPC produce secondary CSH gel which implies a high pozzolanic property of RHA siliceous particles.

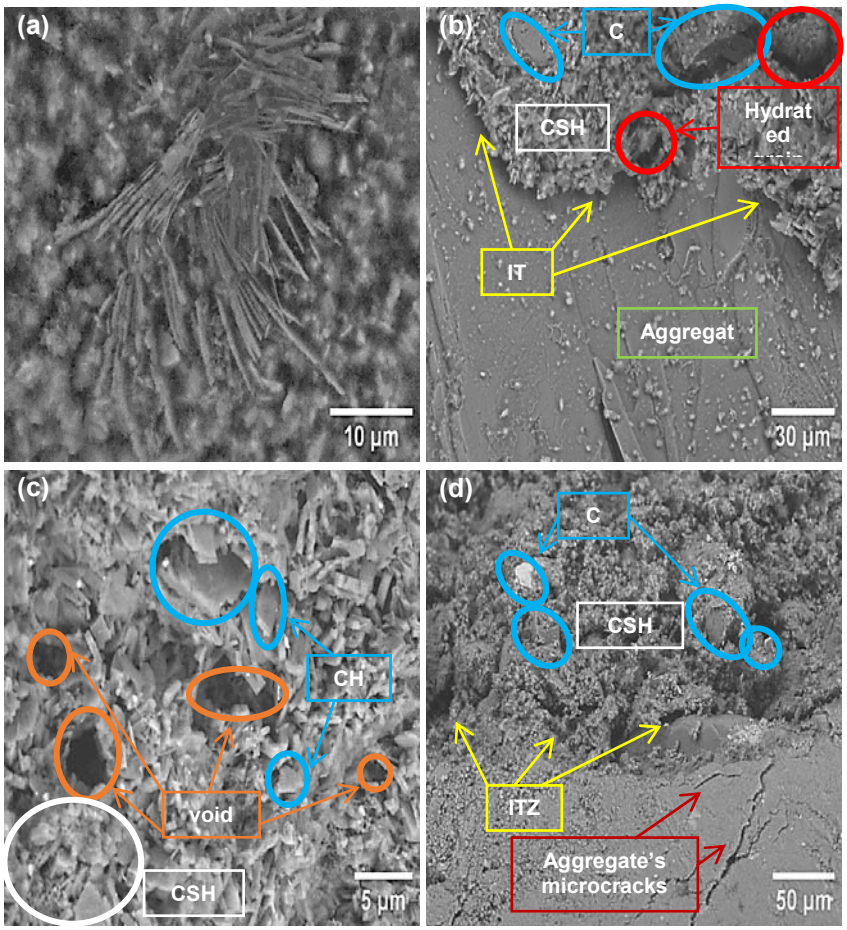


Fig. 3 – RHA-SCC sample microstructures showing: a) formation of ettringite (SC15); b) interfacial transition zone at SC06; c) matrix with reaction gel products (SC11); d) interfacial transition zone at SC05 (Color Online).

## 4. CONCLUSIONS

Experimental works were conducted in this study to investigate the microstructural characterization and strength development of rice husk ash-based self-compacting concrete (RHA-SCC). The following conclusions were presented:

- Various microstructures were observed which supported the results generated in compressive strengths. One is the formation of ettringite seen as needle-like morphology at various lengths. Another is the honeycomb structure inherent to RHA microstructure confirmed a decrease in compressive strength due to the high porosity and specific surface area of RHA. While the milky globular structure revealed the presence of both CSH and CH gel products distinct from the rest of the micrographs, and yielded high compressive strength.
- The ITZ confirmed in various samples resulted from the agglomeration of fine CSH reaction gel, forming against the neighboring aggregate and resulting in wall effect. Overall, the CSH gel reaction improves the compressive strength of the sample.
- Unreacted RHA was also seen in different micrograph samples and yielded lower compressive strengths. This may be prevented by mixing thoroughly the fresh mixture before casting to the mold. This process enhances not only the strength but as well as the pozzolanic reactions of precursors to other cementitious materials.

*Acknowledgements*. FRPP acknowledges the support from the DOST-SEI ASTHRDP-NSC scholarship for the duration of his research. The authors acknowledge the assistance of Dr. Jose Mario A. Diaz for SEM.

REFERENCES

1. J. Paris, J. Roessler, C. Ferraro, H. Deford, and T. Townsend, J. Clean Prod. **121**, 1–18 (2016).
2. E. Aprianti, P. Shafigh, S. Bahri, and J. Farahan, Constr. Build. Mater. **74**, 176–187 (2015).
3. A. Saloma, H. Hanafiah, D. Elysandi, and D. Meykan, AIP Conf. Proc. **1903**, 050013 (2017).
4. H. Xu., and J. Van Deventer, J. Miner Eng. **15**, 1131–1139 (2002).
5. M. de Paula, I. Tinôco, C. Rodrigues, E. da Silva, and C. Souza, Rev. Bras. Eng. Agric. e Ambient **13**, 353–357 (2009).
6. T. Hung, P. Louda, D. Kroisova, O. Bortnovsky, and N. Thang, Adv. Compos. Mater. – Anal. Nat. Man-Made Mater., 2011.
7. L. Li and Y. Feng, Appl. Sci. **11**, 3063 (2021).
8. G. Hu, Q. Yang, X. Qiu, H. Liu, Y. Qian, and S. Xiao, Materials (Basel) **15** (2022).
9. S. Zabihi, H. Tavakoli, and E. Mohseni, J. Mater. Civ. Eng. **30**, 04018183 (2018).
10. W. Xu, T. Lo, S. Memon, Constr. Build. Mater. **29**, 541–547 (2012).
11. G. Barger, J. Bayles, B. Blair, D. Brown, H. Chen *et al.*, Portl. Cem. Assoc., 1–16 (2001).
12. A. Fernández-Jiménez and A. Palomo, A. Cem. Concr. Res., **35**, 1984–1992 (2005).